Composition of C-S-H in pastes with increasing levels of silica fume addition

J.E. Rossen[a]*, B. Lothenbach[b], K.L. Scrivener[a]

[a]*Laboratory of Construction Materials, Ecole Polytechnique Fédérale de Lausanne, Switzerland*

[b] *Empa, Swiss Federal Laboratories for Materials Science and Technology, Laboratory for Concrete and Construction Chemistry, Überlandstrasse 129, 8600 Dübendorf, Switzerland*

*corresponding author, john.rossen@alumni.epfl.ch

Abstract

New results show that the microstructure development of cement-silica fume blends is very different from plain cement. portlandite (CH) tends to precipitate as platelets and even around clinker grains as "CH rims" and is consumed by pozzolanic reaction with silica fume. The Ca/Si ratio in the inner product (IP) C-S-H decreases as CH is consumed to reach Ca/Si ≈ 1.40-1.50 at the point when CH has disappeared, and then drops down to 1.00 in absence of CH. At later ages, the IP C-S-H is often composed of two distinct regions. The outermost (formed first) consists of originally high Ca/Si C-S-H, which Ca/Si slowly decreases. The second (formed later) forms only once CH is no longer present and has a lower Ca/Si. Between 10 and 38°C, the main effect of increasing the temperature is to accelerate the reaction of cement and increase the reactivity of silica fume. The changes in Ca and Si in the pore solution of similar systems suggest that the composition of the solution and the solids reciprocally influence each other.

Keywords: (B) Calcium silicate hydrate (C-S-H); (D) blended cement; (D) silica fume; (B) SEM; (B) TEM

1. Introduction

The main hydrate phases in Portland cement pastes and blends of cement with supplementary cementitious materials (SCMs) are calcium silicate hydrate (C-S-H) and portlandite (CH). The hyphens in C-S-H indicate a variable composition. C-S-H in cementitious binders determines most of the properties of the final material. They include the porosity, the chemical binding capabilities, and the nature and amount of secondary phases, all of which affect the mechanical properties and durability. A basic understanding of this phase, in particular in cement pastes, is essential to better understand the impact of any change in the C-S-H on the final microstructure of cement pastes.

There are two main experimental approaches to study C-S-H. One approach is to synthesise it and equilibrate it in dilute conditions (typically solution/solid ≈ 50), which allows the composition in thermodynamic equilibrium to be established. The other is to characterise C-S-H within a cement paste (with typical water/binder ratios of 0.3-0.7 [1]). Here it is formed by rapid dissolution-precipitation processes but is not straightforward to analyse as it is part of a very heterogeneous microstructure. C-S-H is often referred to as a "gel" as it has little or no long range order (peaks in XRD). However, studies have shown that in both synthetic and paste systems it is made up of nanocrystalline regions with an atomic structure resembling tobermorite and/or jennite [2]. In these minerals and in C-S-H, a central layer of calcium and oxygen is flanked on both sides by tetrahedral silicate chains. These "dreierketten" chains have a repeat unit of three. Two tetrahedra share an oxygen with the Ca-O layer and the third is not directly bound to the Ca-O layer, but "bridges" adjacent paired tetrahedra. The interlayer region contains variable amounts of water and other ions, notably calcium.

One very important characteristic of C-S-H is its variable composition, which is caused by defects and guest ions in its crystal structure. Several mechanisms have been described to allow variation of Ca/Si, although doubts still remain at Ca/Si over 1.50 [2]. It is known that the Ca/Si ratio of the C-S-H varies due to missing bridging silica tetrahedra [3], charge compensation of terminal oxygen atoms by calcium rather than protons and by the likely presence of calcium in the interlayer [4,5]. Aluminium may replace silicon in the bridging tetrahedra and, less commonly, in other sites [6,7]. SCMs generally supply more silica and alumina to the system, thus the final composition of the C-S-H and amount of secondary

51   phases are affected this way. The (alumino-)silicate chains of C-S-H in blended cements condense to

52   form longer chains than non-blended systems [8,9].

53   The possible range of compositions is known for synthetic preparations. Solubility data in the

54   CaO-SiO$_2$-H$_2$O system reports a Ca/Si in C-S-H which can vary from ≈ 0.67 up to ≈ 2.00 depending on

55   the ionic activity of Si and Ca, generally with precipitation of portlandite occurring due to

56   supersaturation of Ca with respect to the solid phase [1,4,10–12]. Pure C-S-H by most synthesis routes

57   only exists for Ca/Si = 1.50 or less, with most attempts to form C-S-H with higher Ca/Si causing the co-

58   precipitation of portlandite [1,4,10–12]. Studies have reported changes in the structure of C-S-H

59   depending on the Ca/Si [3,12–15], on alumina substitution [16–19] and on the dependence of the

60   composition of C-(A-)S-H (C-S-H with or without alumina substitution) to solution composition,

61   temperature and pH [20–23]. On the other hand, the C-S-H which forms with the hydration of plain

62   Portland cement is generally reported to have an average Ca/Si of approximately 1.75, e.g. [24] with

63   lower values generally reported for cement pastes containing supplementary cementitious materials

64   such as slag and fly ash [25–27]. We however lack a more precise idea about the range of possible

65   Ca/Si of C-S-H in pastes. We are therefore interested in exploring this using blends of Portland cement

66   with low to high additions of silica fume. These systems are suitable for this purpose because of the

67   high reactivity of silica fume particles.

68   Silica fume is a highly reactive SCM which typically has a very small size – in the 100s of nm. Its

69   particles are mainly amorphous SiO$_2$. It is added in rather small amounts in practice, typically 5-10%, to

70   reduce bleeding, enhance mechanical properties and improve durability [28]. Higher dosages of silica

71   fume (up to 50%) are used however to investigate low-pH materials, for example [29].

72   Silica fume affects the hydration kinetics. It accelerates the hydration of C$_3$S because it provides more

73   nucleation sites for hydrates to form and grow. This is one aspect of the "filler effect" which is the name

74   given to the physical effect of blending cement with other materials without changing the chemical

75   reactions of the system [30,31]. Silica fume has a particularly strong effect due to its small size.

76   Silica fume can also react with CH to form additional C-S-H. Thermodynamic calculations for a cement

77   containing increasing amounts up to $\approx$ 50% by weight of silica fume [32], assuming complete reaction

78   of both the clinker component and silica fume, show that increasing levels of replacement leads to a

79   decrease in portlandite and the Ca/Si of C-S-H. The lower Ca/Si leads to an increase in alkali uptake

80   which in turn can decrease the pH of the pore solution, which can bring additional changes to the

81   microstructure (see Fig. 5 in [32]).

82   Transmission electron microscopy (TEM) has shown that the morphology of C-S-H in pastes is changed

83   in presence of silica fume in blends hydrated at 40°C [33] to resemble foils which differ from the fibrils

84   observed in PC.

85   Temperature does not appear to affect the Ca/Si in C-S-H from cement [34] nor its morphology [2,35].

86   An increase in temperature can change its density as seen by different grey levels and decrease the

87   bound water content [34]. In blended cements, temperature is expected to act on the kinetics of cement

88   and SCM reaction and can impact the Ca/Si and the Al/Si depending on the degree of reaction of the

89   SCM. The morphology of C-S-H does not appear to differ in blends either, e.g. [26].

90   In this paper new results on the C-S-H composition of real pastes are presented, measured over time in

91   pastes of water/binder = 0.4 by scanning electron microscopy with energy-dispersive spectrometry

92   (SEM-EDS) and compared to the amount of CH determined by thermogravimetric analysis (TGA). This

93   was done for temperatures within the range 10-38°C. The morphology of the outer product (OP) C-S-H

94   at later age was observed in several blends at 20°C by TEM.

95   2. Materials and methods

96   The blends studied are summarized in Table 1. They consisted of a plain Portland cement

97   (CEM I 32.5 R) with undensified silica fume (98.7% SiO_2). In two mixes quartz was also added to

98   increase the water to reactive binder (cement and silica fume) ratio without problems of bleeding. The

99   mixes with quartz were observed only at 90 days of hydration. The phase composition of cement is

100   given in Table 2. The chemical composition by XRF for all the materials is given in Table 3.

101 The cement and quartz were mixed in a Turbula T2F blender for 40 minutes. The silica fume was

102 dispersed in the distilled water using a hand blender for 2-4 minutes to form a slurry. It was set at

103 approximately 12,000 rpm. Each slurry was mixed for an additional 2 minutes just before each sample

104 was cast. The slurry was poured into the cement (or cement and quartz mixture) and mixed for two

105 minutes using a vertical mixer (IKA LABORTECHNIK RW20.n) with a rotation speed of about 1,600

106 rpm. This procedure was sufficient to limit the agglomeration of silica fume particles in the

107 microstructure. Also, all samples were workable without the need for superplasticiser.

108 Samples were cast into 50 ml plastic cylindrical tubes (35 mm diameter and 70 mm high) and then

109 stored first during 24 hours at 10, 20 or 38°C. They correspond to reasonable temperatures used in real

110 conditions and are not expected to destabilise Ettringite [36]. They were then removed from the mould

111 and stored in a second container of slightly larger width (38 mm diameter and 62 mm high). A small

112 amount of additional distilled water was added to maintain the sample under water. The amount of

113 additional water was limited to minimize leaching of the pore solution. They were then stored again at

114 the same respective temperatures.

115

Table 1: Mix design for the cement-silica fume blends

	Cement "PC" [wt%]	Silica fume "SF" [wt%]	Quartz "Q" [wt%]	SF/PC ratio [-]	Water/(PC+SF) ratio [-]	Water/binder ratio [-]
PC	100	-	-	0.00	0.40	0.40
PC(Q) 9.1SF	81.8	9.1	9.1	0.11	0.44	0.40
PC 10SF	90	10	-	0.11	0.40	0.40
PC(Q) 20SF	60	20	20	0.33	0.50	0.40
PC 25SF	75	25	-	0.33	0.40	0.40
PC 45SF	55	45	-	0.82	0.40	0.40

116

117

Table 2: Phase composition of the cement by XRD and Rietveld analysis, in [wt%].

	Alite	Belite	C_3A	C_4AF	CaO	MgO	$CaCO_3$	SiO_2	$CaSO_4$	K_2SO_4
PC	55.2	14.0	10.8	6.2	0.3	1.1	3.3	0.6	5.8	2.6

118

119

Table 3: Chemical composition by XRF, in [wt%].

	SiO_2	Al_2O_3	Fe_2O_3	CaO	MgO	SO_3	Na_2O_3	K_2O	TiO_2	P_2O_5	Mn_2O_3	LOI
PC	21.1	5.6	2.6	64.9	1.6	2.8	0.2	0.9	0.3	0.1	0.1	1.9
Q	98.1	1.1	0.0	-	-	-	0.1	0.6	0.1	0.0	0.0	0.2
SF	98.7	0.3	0.0	0.2	0.0	-	0.1	0.3	0.4	0.0	0.0	0.5

120

121   At different hydration times slices approximately 2 mm thick were cut from the samples using a

122   diamond saw and distilled water as lubricant. The slices were stored five days in isopropanol to remove

123   the water by solvent exchange, with the solution being changed once within the first day to enhance the

124   removal of water. After five days, the samples were stored in a desiccator for several days to evaporate

125   the isopropanol.

126   Samples were ground by hand in a mortar for thermogravimetric analysis. TGA was carried out using a

127   Mettler-Toledo TGA/SDTA 851 balance with a 10°C/min ramp from 30°C to 900°C under a constant

128   30 ml/min flux of nitrogen.

129   For the preparation of SEM samples, a piece of dried paste was cut and impregnated in EPO-TEK 301

130   resin, prepolished using SiC paper (1200 grade) and isopropanol as lubricant, polished using several

131   diamond grades (9, 3 and 1 μm) with deodorised petrol as lubricant, and carbon coated with a layer

132   about 20-30 nm thick using a BAL-TEC CED 030 carbon evaporator. BSE images were taken using a

133   FEI Quanta 200 SEM equipped with a Bruker AXS XFlash 4030 EDS detector for point analysis. Only

134   measurements in IP rims larger than the estimated interaction volume of the electron beam (≈2-3 μm

135   diameter) were taken into consideration. The SEM operating voltage was 15kV. The spot size was

136   adjusted to yield a current of approximately 0.7 nA and an EDS livetime of about 3-4 seconds per point

137   analysis (50'000 total counts per spectrum). PB-ZAF with $\varphi(\rho z)$ matrix corrections were used to

138   quantify a preset list of elements (O, Na, Mg, Al, Si, P, S, Cl, K, Ca, Ti, Fe). The software used a

139   standard database comprised of several relevant oxides such as silica, alumina, jadeite and wollastonite

140   to determine the concentrations of each element. Oxygen was determined by stoichiometry.

141   In parallel work, it was shown [37,38] that the composition of C-S-H measured in SEM-EDS – when

142   represented as a scatter plot (e.g. Si/Ca – Al/Ca) – could be estimated by choosing the value with the

143   least intermixing of C-S-H with CH or other phases rich in calcium. Usually, the Ca/Si value is taken as

144   the edge of the cloud of points (least intermixed points) in a plot of Al/Si against Si/Ca. In the samples

145   studied here, most measurements of OP contained silica fume particles as well as C-S-H [38] within the

146   interaction volume, particularly at high additions of silica fume. Therefore, only measurements from the

147   IP region were taken into consideration. Around 20 points were analysed for each sample. Values of

148   Ca/Si were taken as the average of these analyses and the error given is the standard deviation of these

149   points.

150   Thin lamellae for transmission electron microscopy (TEM) were prepared by taking smaller pieces of

151   dried paste and impregnating them using EMS Embed 812 resin. Each sample was then cut to a thin

152   slice (of dimensions 1.7 mm × 1.7 mm × 0.7 mm) using a WELL diamond wire saw, thinned down

153   mechanically to a bevel by mean of the Tripod method (supplied by ALLIED Tech) to yield a thickness

154   of about 20-30 μm on the thick side. It was then glued to a copper ring, ion-thinned with an Argon PIPS

155   (GATAN Precision Ion Polishing System Model 691) operated at maximum 1.5 keV to achieve electron

156   transparency and coated with a 5 nm layer of carbon using a CRESSINGTON 208 high vacuum carbon

157   coater. As a precaution, samples were coated only prior to observation in the TEM and were always

158   stored in a high vacuum desiccator. TEM observations were carried out using a FEI Tecnai Osiris at an

159   operating voltage of 80 kV in scanning TEM mode (STEM) with EDS mapping. A high spot size and

160   the nanoprobe mode were used to limit the beam current to less than 0.160 nA. Quantification was done

161   using the standardless Cliff-Lorimer ratio technique [39]. It ignores the effects of X-ray absorption and

162   fluorescence inside the material assuming the sample is thin enough. The background is subtracted from

163   the peaks before concentrations C_A and C_B of elements A and B are calculated using the equation

164
$$\frac{C_A}{C_B} = k_{AB} \frac{I_A}{I_B} \qquad (1)$$

165   This equation relates the above-background characteristic intensities I_A and I_B to the concentrations

166   using the factor k_{AB} which depends on the system and the accelerating voltage. Additional details on the

167   procedure can be found in [37] and in [38].

168   The heat of hydration was followed on a series of samples in a Thermometrics TAM Air isothermal

169   calorimeter set at 20°C and located in an air-conditioned room at approximately 20°C. For 10 g of

170   cement paste, 4.14 g of distilled water was used for each channel as a reference as this is of approximate

171 equivalent specific heat. The resulting heat release is normalised to the mass of the paste and the

172 anhydrous clinker content.

## 3. Results and discussion

3.1. Kinetics

175 Figure 1 shows the calorimetry of the blends at 20°C. As widely reported, the reaction of C_3S is

176 strongly accelerated by the presence of silica fume [8,40–42]. The reaction of C_3A occurs earlier and is

177 enhanced [41] due to the adsorption of sulfate on C-S-H. Similar effects were observed at the other

178 temperatures, with an underlying acceleration in all reactions due to temperature.

179
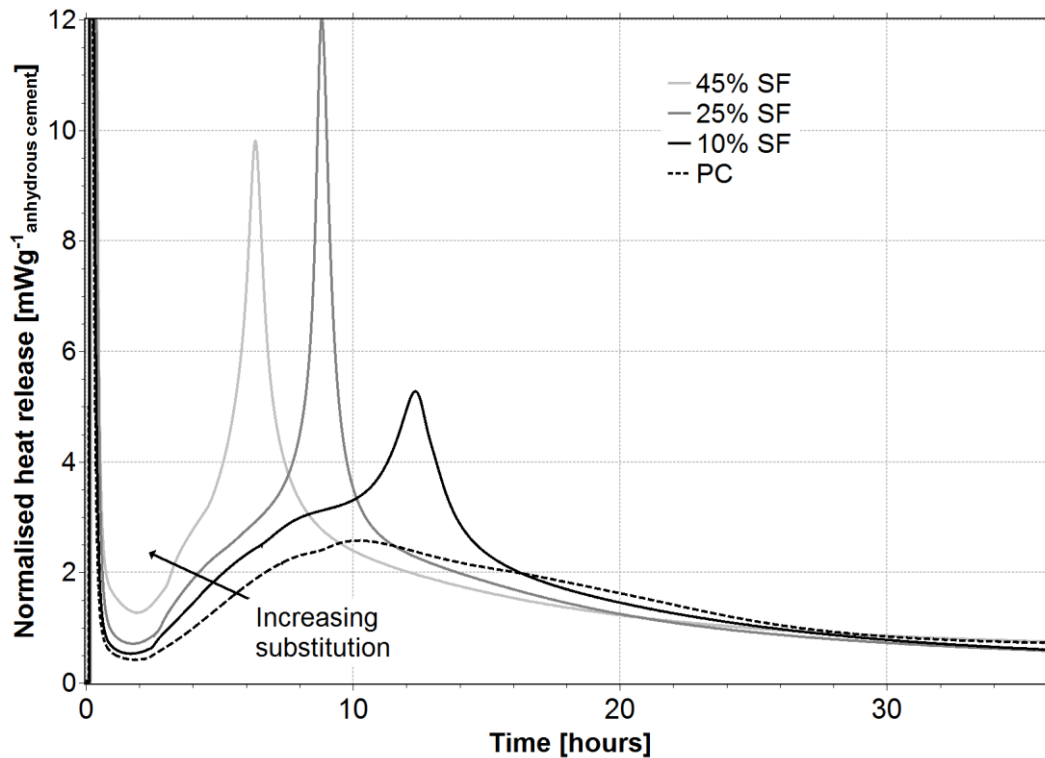
Figure 1: Isothermal calorimetry data for the four systems hydrated at 20°C. The heat release is divided by the anhydrous cement content. 36 hours of hydration are shown.

182 Figure 2 shows the evolution of CH in the different blends. The rate of consumption increases with

183 temperature as expected.
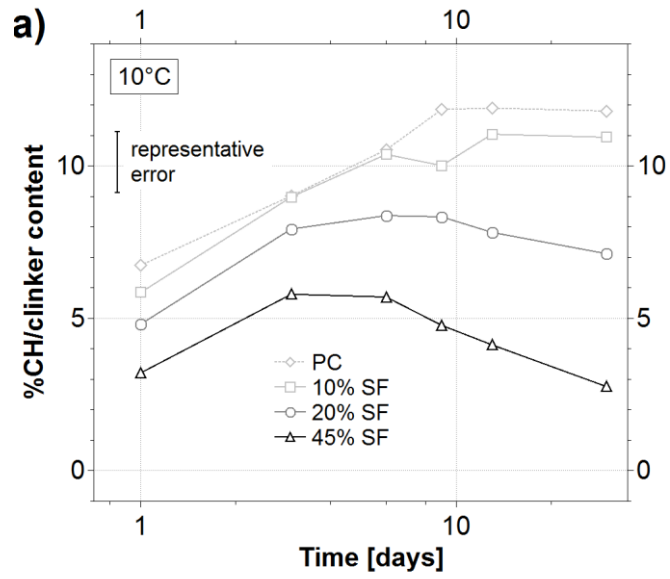
184
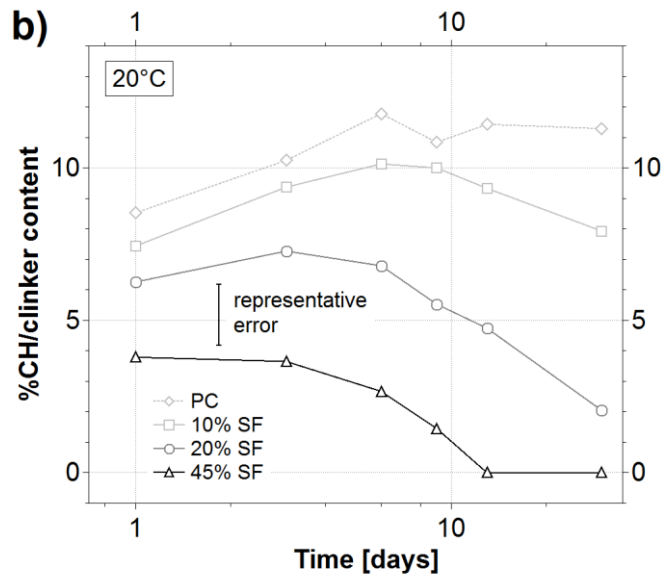
185
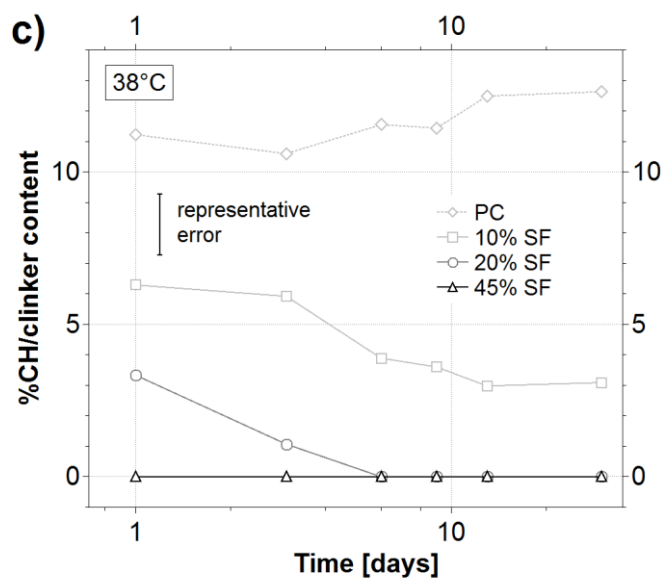
186

187 **Figure 2: %CH normalised to the clinker content for the 3 temperatures. (a) Data from the series hydrated at 10°C, (b)**
188 **20°C and (c) 38°C.**

3.2. Microstructure

190   Figure 3 compares the microstructure of the blends at 20°C after 3 days of hydration. The addition of

191   silica fume seems to accentuate the formation of gaps between the reacting grains and the hydrate shells

192   resulting in more and larger hollow "Hadley" grains from the hydration of small cement grains, as seen

193   for 25% and 45% substitution in Figure 3c and Figure 3d. This may be attributed to the fact that the

194   silica fume particles provide more sites for nucleation resulting in the formation of more "outer" and

195   less "inner" product at early ages. Similarly, the outer product regions appear more homogeneous in the

196   systems with silica fume, reducing the amount of large capillary pores which are still visible in the plain
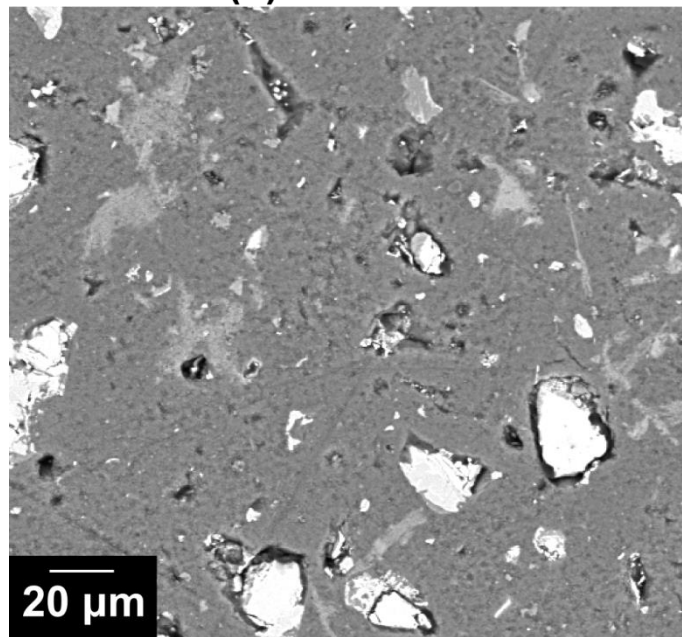
197   cement (Figure 3a).

(a) 100%PC

198

(b) PC-10SF

199
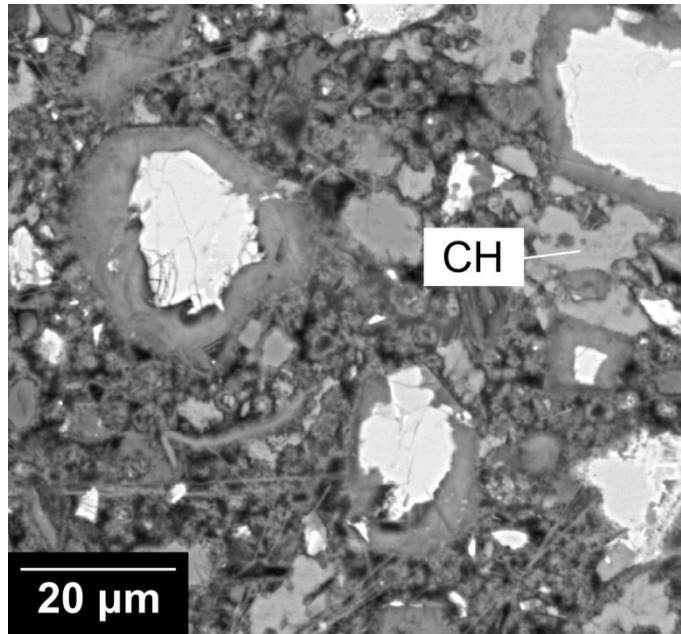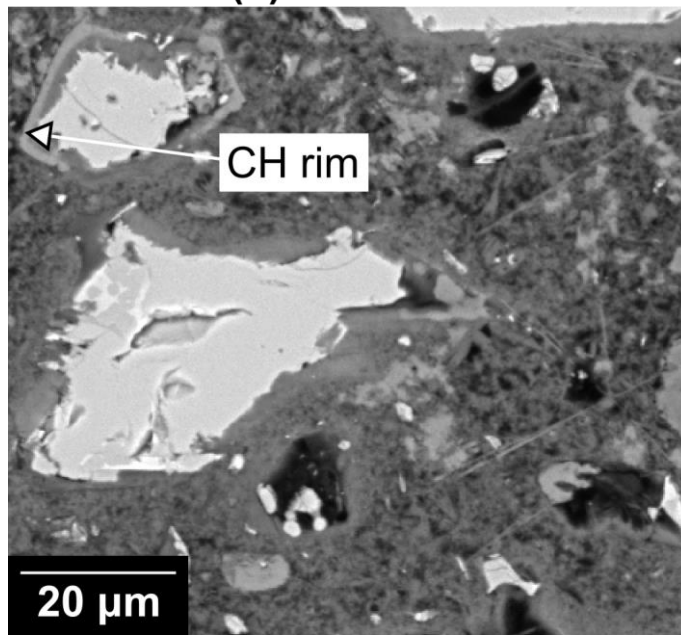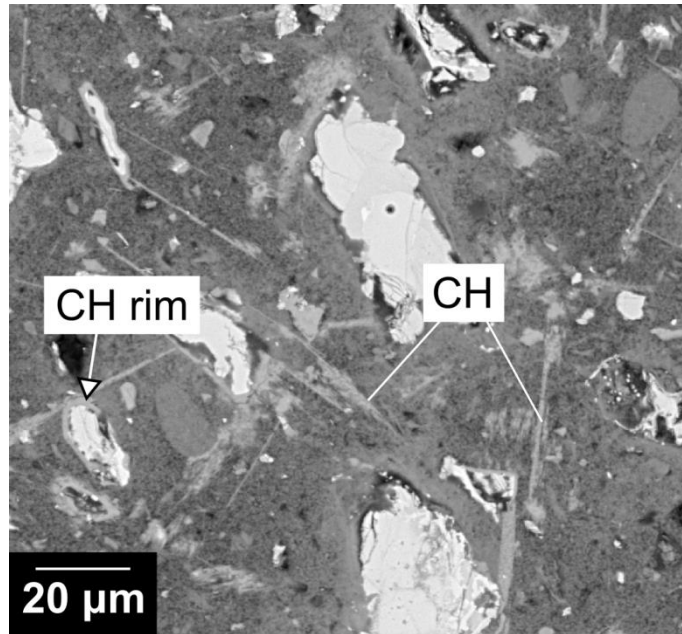
Figure 3: Pastes hydrated at 20°C for 3 days.

Silica fume also impacts the morphology of CH. In the plain cement, CH forms mostly as masses of CH

with a few platelets (Figure 3a). In silica fume blends there are a majority of platelets. These changes in

morphology are more pronounced as the level of silica fume increases. At the higher levels of silica

fume replacement another interesting feature appears for some of the clinker grains. This is the

formation of CH in the gap between the hydration shell and the reacting grain, an example of which is

shown at higher magnification in Figure 4b. It appears that the presence of silica fume particles between

209   the clinker grains makes the precipitation of calcium hydroxide in the outer space difficult (perhaps due

210   to "poisoning" of CH growth [43]), such that the gaps become favourable sites for CH growth. Possible

211   reasons for this are either that the silicate concentration in the gap is lower or that the available space

212   favours the growth of portlandite.

213   In the range of temperatures studied there was a relatively small impact of temperature on the

214   appearance of the microstructures at similar degrees of hydration. In the plain cement system some

215   densification of C-S-H and coarsening of the porosity could be observed as previously reported [34]. In

216   the silica fume blends such changes were less evident.
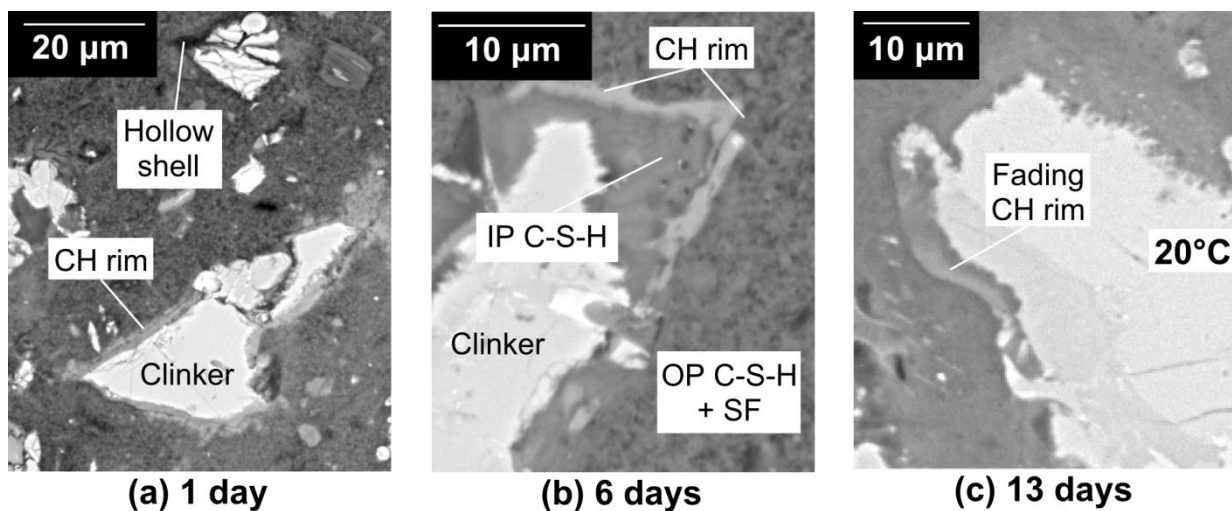
**Figure 4: Microstructure evolution of PC 25SF blend hydrated at 20°C.**

219   After 90 days of hydration many C-S-H rims around the clinker grains showed two distinct grey levels

220   an outer brighter rim (formed first) and a darker inner rim (formed later). They are referred to as "Early

221   IP" and "Later IP". There was considerable variation in the rim thicknesses within any one sample, but

222   a general trend towards thicker darker parts with increasing level of silica fume replacement and

223   increasing temperature. Figure 5 illustrates this range of variation. Figure 6 shows a quantitative EDS

224   map of a two tone rim in the PC(Q) 20SF sample (10°C). Here it is clear that the calcium content (and

225   consequently Ca/Si ratio) in the darker inner part is lower, while the content of silica seems to be

226   similar. It should be noted that this kind of two tone rim is different from that formed in pastes hydrated

227   a two different temperatures [44,45] where the change in grey level results from a change in density

228 rather than chemical compositions as here. The formation of the darker inner rims appears to coincide

229 with the disappearance of calcium hydroxide as a separate phase in the microstructure, at which point a

230 change in either one or both the Si and Ca concentrations in the pore solution will occur. This is

231 supported by two recent examples of analyses of pore solutions from blends with 40% replacement of

232 cement by silica fume where the Si in solution reached a maximum of 1.5 mmol·l^{-1} [46] and 1.04

233 mmol·l^{-1} [47]. This is around ten times greater than the typical concentration seen in a plain cement

234 paste [48].

235

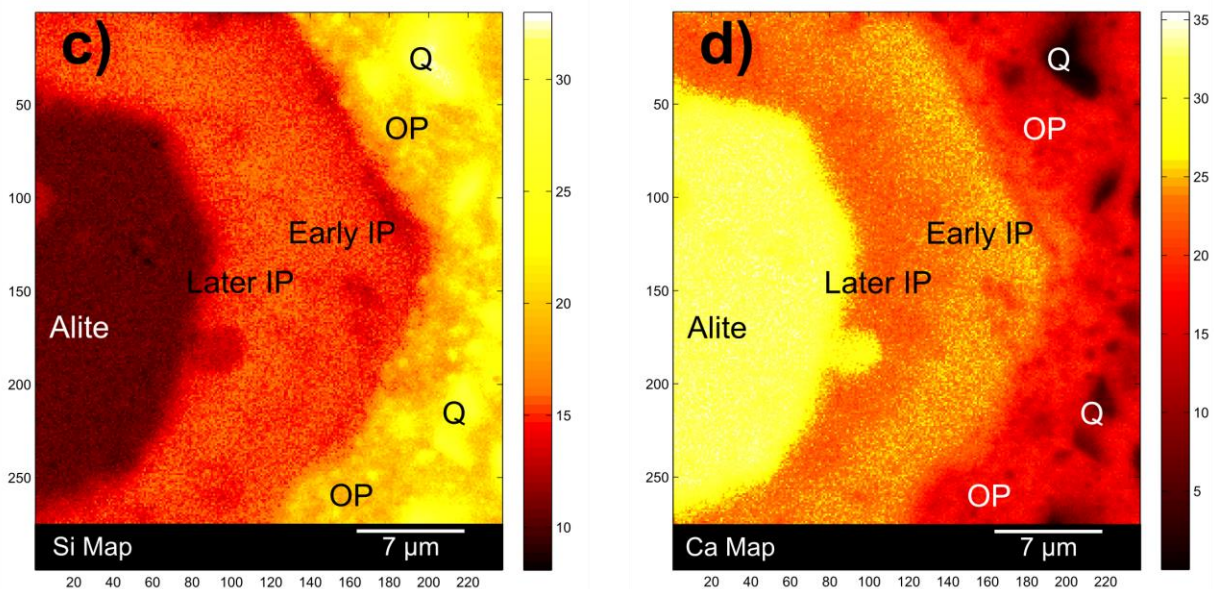**(a)** PC(Q) 9.1SF (20°C)   **(b)** PC(Q) 20SF (20°C)   **(c)** PC 45SF (38°C)
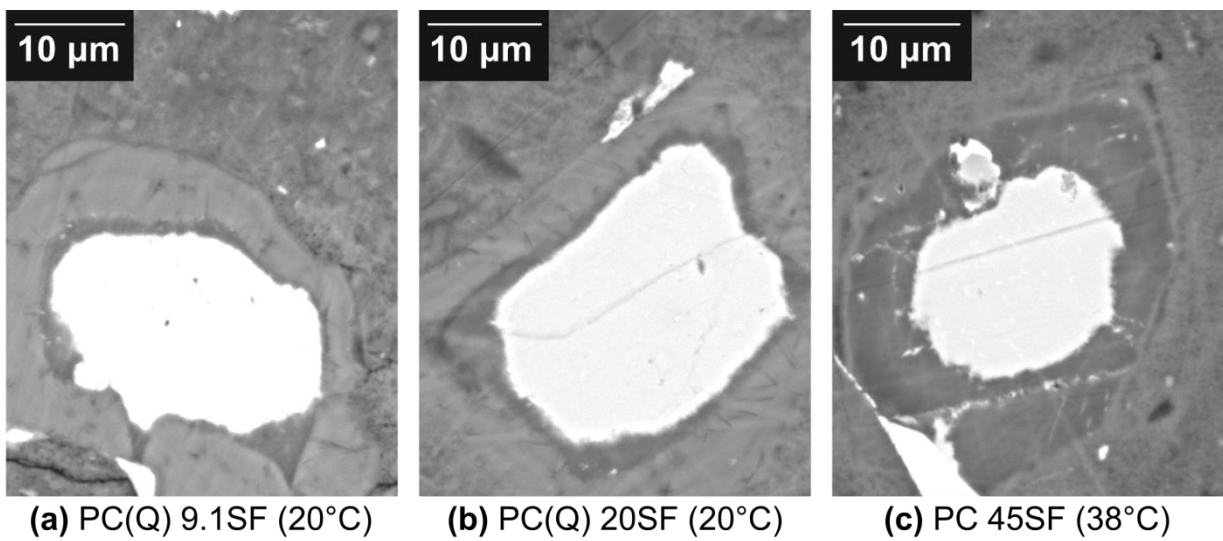
236 **Figure 5: Microstructure of matured samples (hydrated for 90 days) which illustrate the presence of two IP rims of C-**
237 **S-H.**

238
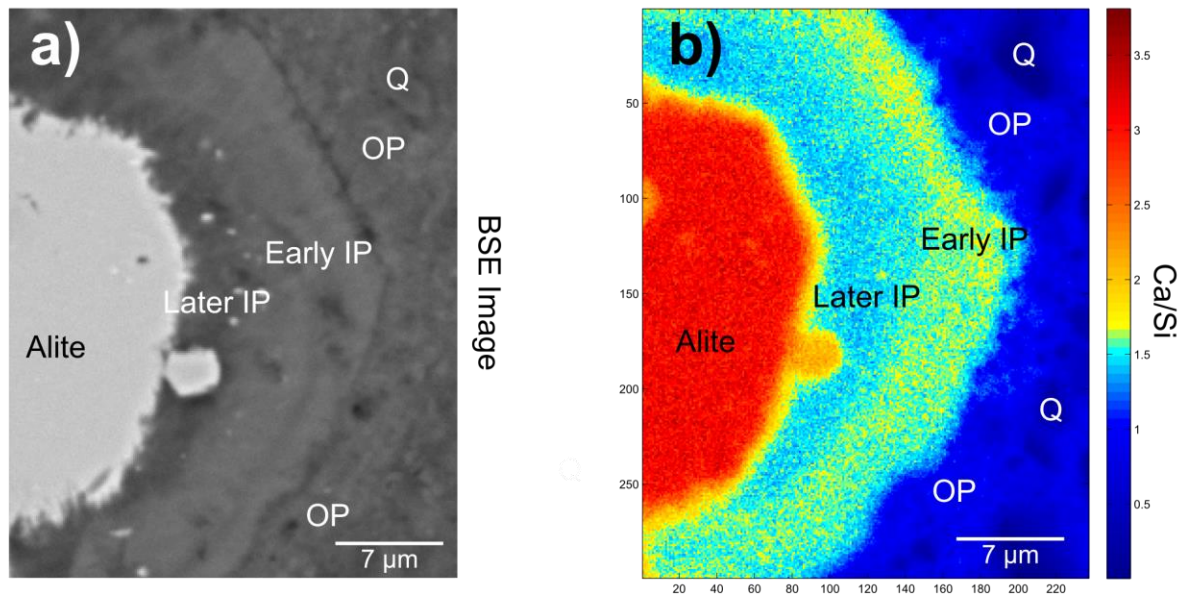
SEM-EDS map of PC(Q) 20SF (10°C)

239

Figure 6: (a) BSE SEM image of an area of the PC(Q) 25SF (10°C) sample analysed by SEM-EDS to map the composition of both the "Early IP" and the "Later IP". (b) The Ca/Si ratio quantified over the whole area. The Early IP has a slightly higher Ca/Si than the Later IP. The bright line between the Alite and Later IP is an edge effect due to the interaction volume. (c) and (d) show the quantified Ca and Si maps respectively.

3.3. C-S-H composition

The Ca/Si ratio measured in 3 month old samples of plain cement was ≈ 2.0 (averaged value from EDS analyses) and did not show any variation with temperature, in agreement with previous results [34]. As expected, the Ca/Si of C-S-H in blends is lower. After 28 days of hydration, in the 10 SF series, the lowest Ca/Si of the inner product was 1.65 ± 0.11 (at 38°C). In the PC 25SF series the lowest value was

15

249   1.25 ± 0.17 (28 days at 38°C) and in the 45% SF blend the lowest value of Ca/Si was 1.00 ± 0.05 (28

250   days at 38°C). Figure 7a shows the Ca/Si of the Early IP C-S-H plotted against the amount of CH

251   relative to the anhydrous cement content for all the samples. In Figure 7b the data for the blends

252   hydrated at 20°C are extracted to show how the Ca/Si values decrease over time. It can be seen that

253   there is a slow decrease to around ≈ 1.40-1.50 while CH remains in the sample. When all the CH is

254   consumed there is a rapid decrease to Ca/Si = 1.00.

255   The lower limit for Ca/Si in presence of CH is broadly consistent with numerous experiments on

256   synthesised C-S-H where the maximum Ca/Si before also precipitating CH is similarly around

257   1.40-1.50 [1,4,10–12]. It can also be seen that there is a tendency towards lower Ca/Si ratios in the

258   blends containing quartz which had a higher water to cementitious (clinker plus silica fume) ratio. This

259   might indicate that greater availability of space facilitates the removal of calcium from the C-S-H as

260   also seen in the work of Bazzoni [49] and Muller [50]. It could also be that the quartz improves the

261   dispersion of silica fume particles due to increased shearing forces, therefore increasing the specific

262   surface area in contact with the pore solution. Silica fume particles would thus be more reactive in

263   presence of quartz particles.

264

265
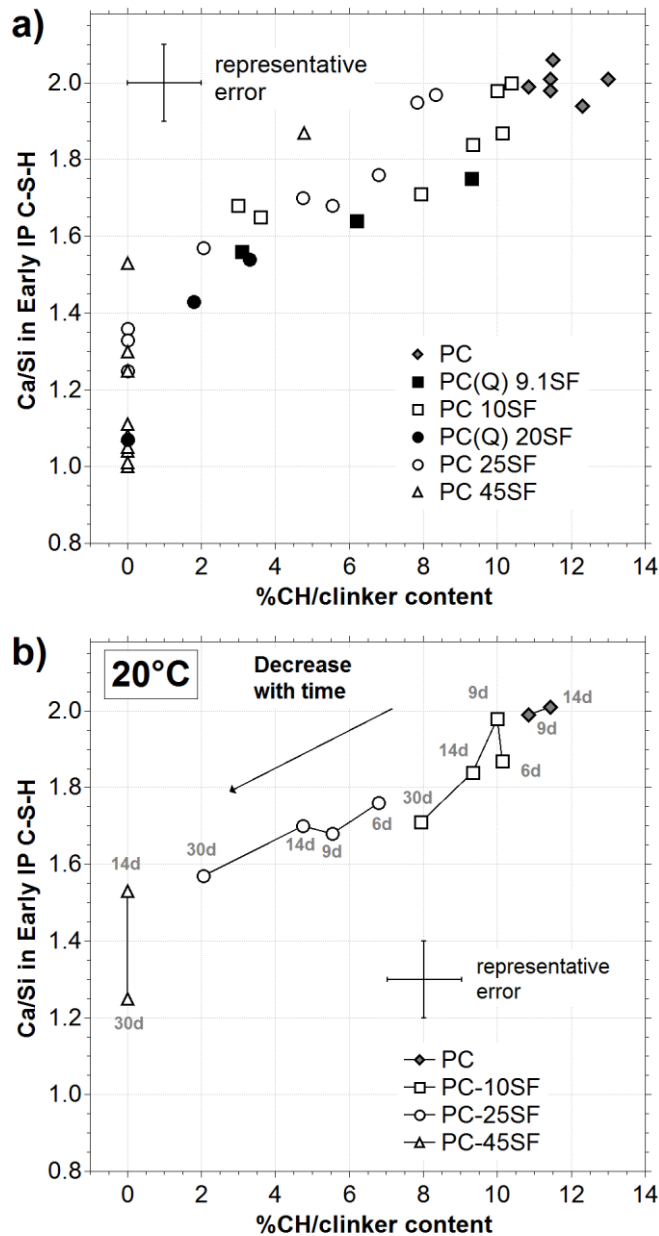
Figure 7: Comparison between the Ca/Si in the Early IP C-S-H and the %CH normalised to clinker content. (a) The data from all series. (b) PC series hydrated at 20°C. The points are connected to show the decrease of Ca/Si with time.

### 3.4. C-S-H morphology

TEM was used to study the morphology of the OP C-S-H in the pastes hydrated at 20°C for 90 days

(Figure 8). Unfortunately, no IP regions from the silica fume blends could be observed due to the small

area thinned for analysis. In the plain cement the morphology of OP C-S-H with Ca/Si = 1.89 is

predominantly fibrillar (Figure 8a) as previously reported [2,51]. The foil like morphology is

predominant in the blends with silica fume (PC 10SF in Figure 8b and PC(Q) 25SF in Figure 8c). This

is compared with the morphology of a C-S-H [52] synthesised at 20°C from CaO and SiO$_2$

275 (water/solid = 45) in a Nitrogen atmosphere and dried with ethanol according to a protocol detailed in

276 [53]. It can be observed that the foil-like morphologies are very similar. It is seen here that the foil-like

277 morphology can exist even in practical paste systems with only 10% silica fume. It is also seen that foil-

278 like morphologies exist in this series with Ca/Si = 1.41 or less. It does not however signify that the

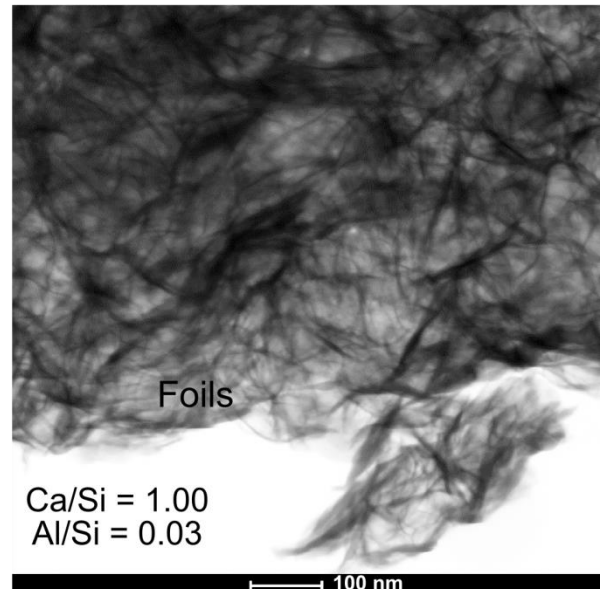279 composition is the only factor determining the morphology.
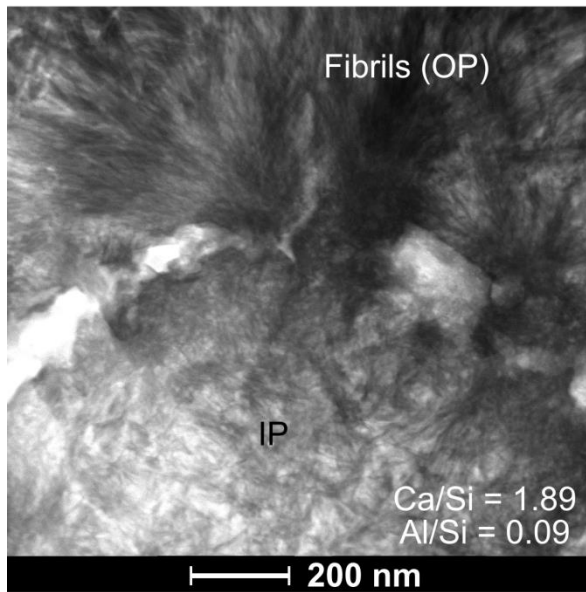
(a) Plain cement (PC), 90 days, 20°C
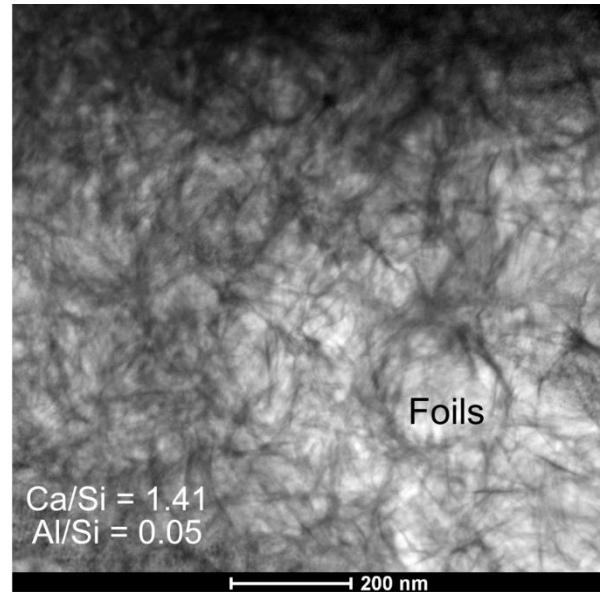
(b) PC 10SF, 90 days, 20°C
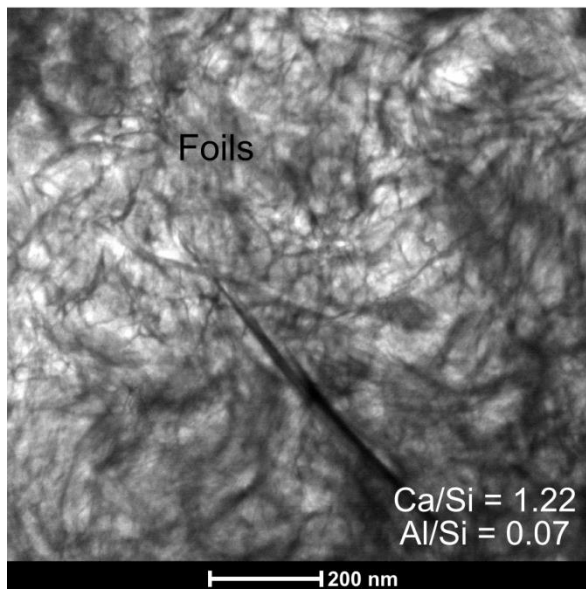
(c) PC(Q) 20SF, 90 days, 20°C

(d) Synthetic C-S-H, 20°C

280

281 **Figure 8: (a) C-S-H of the reference PC sample, 20°C, 90 days (b) PC 10SF, 20°C, 90 days (c) PC(Q) 20SF, 20°C, 90**
282 **days (d) A synthesized C-A-S-H sample with aimed Ca/Si = 1 and Al/Si = 0.03 [52]. The EDS values in pastes are from**
283 **the TEM. The ratios for the synthetic are the aimed values (not measured).**

284   Values of Ca/Si in the IP C-S-H (measured by SEM) and the OP C-S-H (measured by TEM) are

285   compared in Figure 9 for the PC, PC 10SF and PC(Q) 20SF series. The Ca/Si in the plain cement was

286      $\approx$ 1.80-1.90 (taken in SEM from the edge of the cloud of points, not the average), in both the IP and OP.

287   In the series with silica fume, the OP Ca/Si was systematically about 0.2 lower than the Ca/Si of the IP.

288   This is not unexpected as the OP regions are closer to the silica fume particles which supply silica to the

289   system.

290
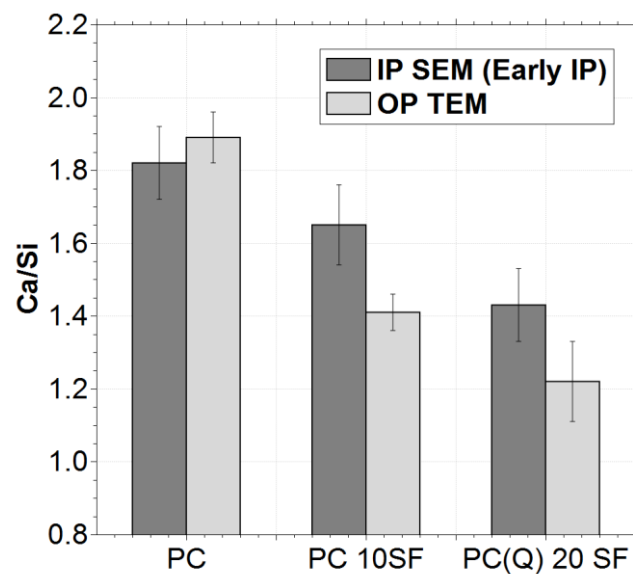
Figure 9: Ca/Si of the C-S-H measured by EDS in the IP (by SEM) and the OP (by TEM).

292   It is interesting to note that despite the Later IP C-S-H being in close proximity to calcium-rich alite, the

293   C-S-H from the Later IP region has a lower Ca/Si then the Early IP. While the formation of C-S-H is

294   affected by the proximity of reactants, it is also affected by the pore solution. The pore solution in plain

295   cement generally remains calcium-rich, which is why in the plain cement, the IP and OP composition

296   are roughly the same. In the silica fume blends, the pore solution is calcium rich at first during the

297   formation of the Early IP but becomes poor in calcium and enriched in silica over time. Then the Later

298   IP C-S-H forms with lower Ca/Si. Over time, the pore solution therefore appears to dominate the

299   formation of C-S-H.

4. Conclusions

The current study presents new results on the microstructure and C-S-H composition of PC-silica fume blends hydrated at 10, 20 and 38°C and with low to high substitution levels.

- The growth morphology of CH is strongly affected by the presence of silica fume which promotes the formation of platelets and even sometimes rims of CH around alite grains.
- It was observed that two rims of IP C-S-H exist in such blends. There was an outer rim ("Early IP") forming first, followed by a darker grey rim ("Later IP") forming at a later stage when the CH was depleted.
- The Ca/Si of the Early IP C-S-H decreases to ≈ 1.40-1.50 as CH is consumed by silica fume. It can drop down to 1.00 in absence of CH.
- The OP C-S-H morphology is foil-like in silica fume blends even with only 10% addition.

These observations suggest the following. At early times, when CH is still present, Ca-rich C-S-H forms. At later age, when more SiO_2 has reacted (and less CH is present), Si-rich C-S-H forms but the Ca/Si ratio of the earlier formed C-S-H also decreases. The loss of calcium from the C-S-H is driven by the consumption of calcium by the reaction of silica fume. It occurs relatively gradually while solid CH is present to replenish calcium to the pore solution and then decrease dramatically when solid CH has all been consumed. This corresponds to changes in the pore solution reported elsewhere [46,47] where a decrease in the Ca concentration and pH is observed, and where an increase of the Si concentration is also observed. This indicates that the composition of the solution and that of the solids reciprocally influence each other.

5. Acknowledgments

6. References

[1] Taylor, H.F.W., Cement Chemistry, 2nd ed., Thomas Telford, 1997.

[2] I.G. Richardson, Tobermorite/jennite-and tobermorite/calcium hydroxide-based models for the structure of C–S–H: applicability to hardened pastes of tricalcium silicate,[beta]-dicalcium silicate, Portland cement, and blends of Portland cement with blast-furnace slag, metakaolin, or silica fume, Cem. Concr. Res. 34 (2004) 1733–1777.

[3] P. Yu, R.J. Kirkpatrick, B. Poe, P.F. McMillan, X. Cong, Structure of calcium silicate hydrate C–S–H Near-, Mid-, and Far-Infrared Spectroscopy, J. Am. Ceram. Soc. 82 (1999) 742–748.

[4] A. Nonat, X. Lecoq, The structure, stoichiometry and properties of C–S–H prepared by C3S hydration under controlled conditions, in: Nucl. Magn. Reson. Spectrosc. Cem.-Based Mater., Springer, Berlin, 1998: pp. 197–207.

[5] A. Nonat, The structure and stoichiometry of C–S–H, Cem. Concr. Res. 34 (2004) 1521–1528.

[6] I.G. Richardson, G.W. Groves, The incorporation of minor and trace elements into calcium silicate hydrate (C–S–H) gel in hardened cement pastes, Cem. Concr. Res. 23 (1993) 131–138.

[7] M.D. Andersen, H.J. Jakobsen, J. Skibsted, Incorporation of aluminum in the calcium silicate hydrate (C–S–H) of hydrated Portland cements: a High-Field 27Al and 29Si MAS NMR investigation, Inorg. Chem. 42 (2003) 2280–2287.

[8] Z.-Q. Wu, J.F. Young, The hydration of tricalcium silicate in the presence of colloidal silica, J. Mater. Sci. 19 (1984) 3477–3486.

[9] D.H. Justnes, Kinetics of reaction in cementitious pastes containing silica fume as studied by 29Si MAS NMR, in: D.P. Colombet, P.H. Zanni, D.A.-R. Grimmer, P.P. Sozzani (Eds.), Nucl. Magn. Reson. Spectrosc. Cem.-Based Mater., Springer Berlin Heidelberg, 1998: pp. 245–268.

[10] S.A. Greenberg, T.N. Chang, Investigation of the colloidal hydrated calcium silicates. II. Solubility relationships in the calcium oxide-silica-water system at 25°, J Phys Chem. 69 (1965) 182–188.

[11] X. Cong, R. Kirkpatrick, Si MAS NMR study of the structure of calcium silicate hydrate, Adv. Cem. Based Mater. 3 (1996) 144–156.

[12] J.J. Chen, J.J. Thomas, H.F.W. Taylor, H.M. Jennings, Solubility and structure of calcium silicate hydrate, Cem. Concr. Res. 34 (2004) 1499–1519.

[13] I. Klur, B. Pollet, J. Virlet, A. Nonat, C-S-H structure evolution with calcium content by multinuclear NMR, in: D.P. Colombet, P.H. Zanni, D.A.-R. Grimmer, P.P. Sozzani (Eds.), Nucl. Magn. Reson. Spectrosc. Cem.-Based Mater., Springer Berlin Heidelberg, 1998: pp. 119–141.

[14] K. Garbev, M. Bornefeld, G. Beuchle, P. Stemmermann, Cell dimensions and composition of nanocrystalline calcium silicate hydrate solid solutions. Part 2: X-Ray and thermogravimetry study, J. Am. Ceram. Soc. 91 (2008) 3015–3023.

[15] K. Garbev, G. Beuchle, M. Bornefeld, L. Black, P. Stemmermann, Cell dimensions and composition of nanocrystalline calcium silicate hydrate solid solutions. Part 1: Synchrotron-based X-ray diffraction, J. Am. Ceram. Soc. 91 (2008) 3005–3014.

[16] P. Faucon, A. Delagrave, C. Richet, J.M. Marchand, H. Zanni, Aluminum incorporation in calcium silicate hydrates (C–S–H) depending on their Ca/Si ratio, J. Phys. Chem. B. 103 (1999) 7796–7802.

[17] G. Renaudin, J. Russias, F. Leroux, F. Frizon, C. Cau-dit-Coumes, Structural characterization of C-S-H and C-A-S-H samples-Part I: Long-range order investigated by Rietveld analyses, J. Solid State Chem. 182 (2009) 3312–3319.

[18] G. Renaudin, J. Russias, F. Leroux, C. Cau-dit-Coumes, F. Frizon, Structural characterization of C-S-H and C-A-S-H samples-Part II: Local environment investigated by spectroscopic analyses, J. Solid State Chem. 182 (2009) 3320–3329.

[19] X. Pardal, I. Pochard, A. Nonat, Experimental study of Si-Al substitution in calcium-silicate-hydrate (C-S-H) prepared under equilibrium conditions, Cem. Concr. Res. 39 (2009) 637–643.

[20] P. Faucon, T. Charpentier, A. Nonat, J.C. Petit, Triple-Quantum two-dimensional 27Al Magic Angle Nuclear Magnetic Resonance study of the aluminum incorporation in calcium silicate hydrates, J. Am. Chem. Soc. 120 (1998) 12075–12082.

[21] R. Barbarulo, H. Peycelon, S. Leclercq, Chemical equilibria between C–S–H and ettringite, at 20 and 85 °C, Cem. Concr. Res. 37 (2007) 1176–1181.

378   [22] I. Garcia Lodeiro, A. Fernández-Jimenez, A. Palomo, D.E Macphee, Effect on fresh C–S–H gels of
379   the simultaneous addition of alkali and aluminium, Cem. Concr. Res. 40 (2010) 27–32.
380   [23] X. Pardal, F. Brunet, T. Charpentier, I. Pochard, A. Nonat, Al-27 and Si-29 solid-state NMR
381   characterization of calcium-aluminosilicate-hydrate, Inorg. Chem. 51 (2012) 1827–1836.
382   [24] I.G. Richardson, The nature of C–S–H in hardened cements, Cem. Concr. Res. 29 (1999) 1131–
383   1147.
384   [25] I.G. Richardson, G.W. Groves, Microstructure and microanalysis of hardened cement pastes
385   involving ground granulated blast-furnace slag, J. Mater. Sci. 27 (1992) 6204–6212.
386   [26] A.V. Girão, I.G. Richardson, R. Taylor, R.M.D. Brydson, Composition, morphology and
387   nanostructure of C–S–H in 70% white Portland cement-30% fly ash blends hydrated at 55 °C.,
388   Cem. Concr. Res. 40 (2010) 1350–1359.
389   [27] F. Deschner, B. Lothenbach, F. Winnefeld, J. Neubauer, Effect of temperature on the hydration of
390   Portland cement blended with siliceous fly ash, Cem. Concr. Res. 52 (2013) 169–181.
391   [28] T.C. Holland, United States, Federal Highway Administration, Silica fume user's manual, Federal
392   Highway Administration, Washington, D.C., 2005.
393   [29] B. Lothenbach, G. Le Saout, M. Ben Haha, R. Figi, E. Wieland, Hydration of a low-alkali CEM
394   III/B–SiO2 cement (LAC), Cem. Concr. Res. 42 (2012) 410–423.
395   [30] W.A. Gutteridge, J.A. Dalziel, Filler cement: The effect of the secondary component on the
396   hydration of Portland cement: Part I. A fine non-hydraulic filler, Cem. Concr. Res. 20 (1990) 778–
397   782.
398   [31] E. Berodier, K. Scrivener, Understanding the filler effect on the nucleation and growth of C-S-H, J.
399   Am. Ceram. Soc. (2014).
400   [32] B. Lothenbach, K. Scrivener, R.D. Hooton, Supplementary cementitious materials, Cem. Concr.
401   Res. 41 (2011) 1244–1256.
402   [33] G.W. Groves, S.A. Rodger, The hydration of C3S and ordinary Portland cement with relatively
403   large additions of micro silica, Adv. Cem. Res. 2 (1989) 135–140.
404   [34] E. Gallucci, X. Zhang, K.L. Scrivener, Effect of temperature on the microstructure of calcium
405   silicate hydrate (C-S-H), Cem. Concr. Res. 53 (2013) 185–195.
406   [35] A.V. Girão, I.G. Richardson, C.B. Porteneuve, R.M.D. Brydson, Composition, morphology and
407   nanostructure of C-S-H in white Portland cement pastes hydrated at 55 °C, Cem. Concr. Res. 37
408   (2007) 1571–1582.
409   [36] B. Lothenbach, T. Matschei, G. Möschner, F.P. Glasser, Thermodynamic modelling of the effect of
410   temperature on the hydration and porosity of Portland cement, Cem. Concr. Res. 38 (2008) 1–18.
411   [37] J.E. Rossen, K.L. Scrivener, Optimisation of SEM-EDS to determine C-S-H composition in
412   matured cement paste samples, in preparation for Mater. Characterisation. (2015).
413   [38] J.E. Rossen, Composition and morphology of C-A-S-H in pastes of alite and cement blended with
414   supplementary cementitious materials, EPFL Thesis n°6294, 2014.
415   [39] D.B. Williams, C.B. Carter, Transmission Electron Microscopy: A Textbook for Materials Science,
416   Springer Science & Business Media, 2009.
417   [40] W. Kurdowski, W. Nocuń-Wczelik, The tricalcium silicate hydration in the presence of active
418   silica, Cem. Concr. Res. 13 (1983) 341–348.
419   [41] H. Cheng-yi, R.F. Feldman, Hydration reactions in portland cement-silica fume blends, Cem.
420   Concr. Res. 15 (1985) 585–592.
421   [42] C.M. Dobson, D.G.C. Goberdhan, J.D.F. Ramsay, S.A. Rodger, 29Si MAS NMR study of the
422   hydration of tricalcium silicate in the presence of finely divided silica, J. Mater. Sci. 23 (1988)
423   4108–4114.
424   [43] Z.-Q. Wu, J.F. Young, Formation of Calcium Hydroxide from Aqueous Suspensions of Tricalcium
425   Silicate, J. Am. Ceram. Soc. 67 (1984) 48–51.
426   [44] C. Famy, K.L. Scrivener, A.K. Crumbie, What causes differences of C-S-H gel grey levels in
427   backscattered electron images?, Cem. Concr. Res. 32 (2002) 1465–1471.
428   [45] K.L. Scrivener, Backscattered electron imaging of cementitious microstructures: understanding and
429   quantification, Cem. Concr. Compos. 26 (2004) 935–945.
430   [46] T.T.H. Bach, C.C.D. Coumes, I. Pochard, C. Mercier, B. Revel, A. Nonat, Influence of temperature
431   on the hydration products of low pH cements, Cem. Concr. Res. 42 (2012) 805–817.

432 [47] B. Lothenbach, D. Rentsch, E. Wieland, Hydration of a silica fume blended low-alkali shotcrete
433   cement, Phys. Chem. Earth Parts ABC. 70–71 (2014) 3–16.
434 [48] B. Lothenbach, F. Winnefeld, C. Alder, E. Wieland, P. Lunk, Effect of temperature on the pore
435   solution, microstructure and hydration products of Portland cement pastes, Cem. Concr. Res. 37
436   (2007) 483–491.
437 [49] A. Bazzoni, Study of early hydration mechanisms of cement by means of electron microscopy,
438   EPFL Thesis n°6296, 2014.
439 [50] A. Muller, Porosity characterisation across different cementitious binders by a multi-technique
440   approach, EPFL Thesis n°6339, 2014.
441 [51] I.G. Richardson, G.W. Groves, Microstructure and microanalysis of hardened ordinary Portland
442   cement pastes, J. Mater. Sci. 28 (1993) 265–277.
443 [52] E. L'Hôpital, B. Lothenbach, G. Le Saout, D. Kulik, K. Scrivener, Incorporation of aluminium in
444   calcium silicate hydrates, Cem. Concr. Res. (2014).
445   http://dx.doi.org/10.1016/j.cemconres.2015.04.007.
446 [53] É. L'Hôpital, Aluminium and alkali uptake in calcium silicate hydrates (C-S-H), EPFL Thesis n°
447   6389, 2014.
448